2026 IEEE/SICE International Symposium on System Integration (SII)
January 11-14, 2026. Cancún, México

Improving the Accuracy of Dynamic Model Identification for Moving Industrial Robots using Indirect Z-direction Vibration Analysis

Ali Khishtan[1], Jihyun Lee*[1]

Abstract— **With the growing use of industrial robots in high-force operations, accurate dynamic modelling has become increasingly critical for their design and control. The authors previously proposed a novel automated method to identify joint dynamic parameters of moving industrial robots, considering frictional behavior across a large portion of the workspace. This method excites the robot using a "*fast chirp*" centrifugal force, allowing precise control of the excitation force. However, its accuracy is limited due to the neglect of out-of-plane *z*-dynamics and the error in the input force model. This paper addresses these limitations to enhance the model's prediction accuracy. Theoretical and experimental excitation forces are compared to assess their influence on identification. The indirect *z*-direction vibration response is formulated accounting for the cross-couplings and analyzed to enhance the prediction accuracy of out-of-plane *z*-dynamics. The experimental results show that the proposed approach reduces prediction error by up to 49.8% compared to the previously identified model, in which the z-direction vibration responses were not considered.**

I. Introduction

Robot modelling for high-force manufacturing processes such as machine tending, milling, and drilling requires accurate dynamic parameters to compensate for joint deflection or control vibrations, enabling high accuracy and speed [1,2]. However, moving robots exhibit highly nonlinear dynamics [3] due to pose- and speed-dependent variations in joint stiffness, damping, and friction, influenced by factors such as lubrication distribution and temperature [4]. Speed changes also alter frictional behavior, affecting modal damping [5]. These effects make it difficult to obtain parameters valid across the entire workspace. An automated identification method is therefore needed to rapidly capture joint dynamics at multiple locations while the robot is in motion.

Different automated identification methods have been investigated [6-11]. Using the robot joint motors is a common way to excite the robot [6,7], but it faces limited bandwidth. External actuators have also been investigated to generate the excitation [8,9], but they are generally limited to static-case identification or single-direction excitation. Operational Modal Analysis (OMA) is another automated identification method [10,11] that utilizes the cutting force as the excitation source. This approach requires actual cutting and depends on the level of process noise during operation; hence, it lacks precise control over the excitation force.

[1] Department of Mechanical and Manufacturing Engineering, University of Calgary, Calgary, AB T2N1N4 Canada (phone: 403-220-6948; fax: 403-282-8406; e-mail: jihyun.lee@ ucalgary.ca).

To address these identification requirements, the authors previously proposed a novel automated method for identifying joint dynamic parameters of moving industrial robots [12]. The method uses a "*fast chirp*" excitation, which is a chirp centrifugal force generated by a customized offset mass tool over a short duration, allowing precise control of the excitation. During identification, the robot moves continuously, and simultaneous two directional chirp excitation in the *x* and *y* axes is applied at multiple zones, enabling rapid coverage of a large workspace in a single test while capturing the frictional behavior of moving joints. However, this method has a limitation because the centrifugal force acts only in the *x*-*y* plane, the robot cannot be directly excited in the local *z*-direction. In the previous work, *z*-direction dynamics were not identified, reducing the model's ability to predict *z*-direction behavior. Local *z*-direction dynamics are critical in processes involving high external forces in that direction, such as robotic drilling [13], and are also necessary for accurate three-dimensional chatter stability prediction in robotic milling [14,15].

This paper extends the proposed identification method to predict *z*-direction dynamics and vibration from multidirectional excitation by using cross couplings in robot dynamics. A new formulation is developed to assess the influence of considering indirectly induced *z*-direction vibrations on model identification accuracy and is validated experimentally. The paper also examines discrepancies between mathematically modelled and experimentally measured excitation forces across the experimental frequency range, and their effect on normalized vibrations. To improve identification accuracy, normalized vibrations are computed using both mathematically derived and experimentally measured forces, and are then compared with reference values from a quasi-static impact hammer test and the developed formulation for simultaneous multidirectional excitation.

This paper is structured as follows: Section II presents the methodology of the proposed approach and introduces the experimental setup and mathematical formulations, including vibration responses and *z*-dynamics. The input force investigation and parameter identification including *z*-direction vibration are presented in Section III. Section IV discusses the validation of vibration responses, the identified model, and the *z*-dynamics prediction. A brief conclusion is provided in Section V.

978-1-6654-5784-2/26/$31.00 ©2026 IEEE

II. METHODOLOGY

A. Experimental Setup for Fast Chirp Identification Method including a Load Cell

The proposed method is implemented using a Staubli RX160 industrial robot, as shown in Fig. 1. The robot moves continuously along a predefined identification trajectory to capture the frictional behaviour of moving joints and its effect on dynamics. Multiple zones along the trajectory are excited by the frequency sweep of a custom-designed offset mass tool driven by a Hiteco QN-1F 6.5/18 24 spindle. During each excitation, the spindle speed follows a chirp signal sweeping linearly from zero to the maximum frequency, imposing a force at the tool tip similar to that experienced during cutting. To minimize model linearization error due to posture changes, each excitation is completed within 4 seconds, and is therefore termed "*fast chirp*" excitation.

The input excitation force is determined by the design of the customized offset mass tool and the selected frequency range and maximum frequency. The tool consists of a cylindrical stem connected to the tool holder, with an offset mass rigidly attached. The frequency range and maximum frequency are first defined. Since the primary vibration modes of the robot lie below 30 Hz [12], the maximum frequency is set to 40 Hz. The equation for the chirp centrifugal force vector $F(t)$ is shown in (1).

$$F(t)=\begin{bmatrix}F_x\\F_y\end{bmatrix}=\underbrace{mr\omega^2}_{A}\begin{bmatrix}\sin(\theta(t))\\\sin(\theta(t)-\pi/2)\end{bmatrix},\ \theta(t)=\int_0^t\omega(s)ds \tag{1}$$

where A is the frequency-dependent force magnitude in each direction, proportional to offset mass m, offset distance r, and spindle frequency ω. The phase shift between the x and y force directions is $-\pi/2$. Once ω is set, m and r are chosen to provide sufficient low-frequency force while avoiding damage to the robot joints and spindle at higher frequencies, as detailed in [12]. In this study, an Omega ATI 160 F/T load cell is also installed on the robot to measure the excitation force directly. The measured force is used in the identification and compared with results obtained using the mathematical input force in (1).

The excited vibration is measured by a PCB 356B18 tri-axial accelerometer. Both the measured output acceleration and the input force are computed at the tool tip using transformation matrices and the acceleration rules for moving rigid bodies, accounting for sensor locations. The acceleration is then converted to displacement in the frequency domain. Since the tool, tool holder, spindle, and load cell are much more rigid than the robot structure, they are modelled as rigid bodies. To enable prediction of z-direction dynamics in the local tool frame, all analyses are carried out in Cartesian space and tool coordinates, with the frame rigidly attached to the spindle as shown in Fig. 1. Once the input and output are obtained, the joint dynamic parameters, namely stiffness and damping, are identified using the method described in the following sections.

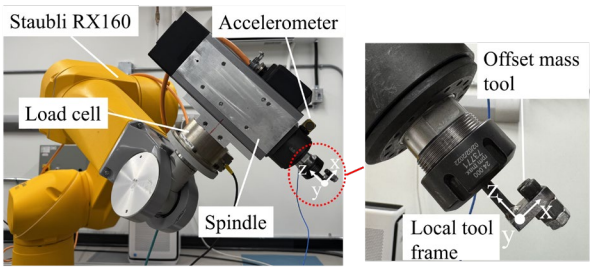

Figure 1. Experimental setup and customized offset mass tool.

B. Mathematical Formulation of Three-dimensional Vibration Responses and Z-direction Dynamics

This study aims to improve model prediction accuracy by capturing z-direction dynamics. The experimental vibration response in the z-direction is incorporated into the analysis, and its dynamics are investigated in both the robot model and the identification process. In industrial robots, cross FRFs, which relate vibration in one direction to excitation in another, are important due to their magnitudes often being comparable to the corresponding direct FRFs [16]. Therefore, the direct FRFs defined in x, y and z directions as H_{xx}, H_{yy}, and H_{zz}, respectively, and the cross FRFs H_{xy}, H_{xz}, H_{yx}, H_{yz}, H_{zx}, and H_{zy} are used in this study. The magnitude of these transfer functions is shown with $\|$ symbol and the phases are shown by $\angle$. Because the centrifugal force provides simultaneous excitation in two directions, the FRFs cannot be directly extracted from the fast-chirp experiments. Instead, the identification process uses the normalized vibration responses in each direction. Accordingly, taking into account both direct and cross FRFs, the normalized frequency-domain vibration displacements in the x, y, and z directions, resulting from excitation forces F_x and F_y in the x and y directions, are calculated in (2) as X/A, Y/A, and Z/A, where j denotes the imaginary unit.

$$\begin{aligned}
\frac{X}{A}(j\omega)&=\frac{X_{Fx}(j\omega)+X_{Fy}(j\omega)}{A}=\begin{bmatrix}|H_{xx}|\\|H_{xy}|\\|H_{xx}|\\|H_{xy}|\end{bmatrix}^{\mathrm{T}}\begin{bmatrix}\cos(\angle H_{xx})\\\cos(\angle H_{xy}-\pi/2)\\j\sin(\angle H_{xx})\\j\sin(\angle H_{xy}-\pi/2)\end{bmatrix}\\
\frac{Y}{A}(j\omega)&=\frac{Y_{Fx}(j\omega)+Y_{Fy}(j\omega)}{A}=\begin{bmatrix}|H_{yy}|\\|H_{yx}|\\|H_{yy}|\\|H_{yx}|\end{bmatrix}^{\mathrm{T}}\begin{bmatrix}\cos(\angle H_{yy})\\\cos(\angle H_{yx}+\pi/2)\\j\sin(\angle H_{yy})\\j\sin(\angle H_{yx}+\pi/2)\end{bmatrix}\\
\frac{Z}{A}(j\omega)&=\frac{Z_{Fx}(j\omega)+Z_{Fy}(j\omega)}{A}=\begin{bmatrix}|H_{zx}|\\|H_{zy}|\\|H_{zx}|\\|H_{zy}|\end{bmatrix}^{\mathrm{T}}\begin{bmatrix}\cos(\angle H_{zx})\\\cos(\angle H_{zy}-\pi/2)\\j\sin(\angle H_{zx})\\j\sin(\angle H_{zy}-\pi/2)\end{bmatrix}
\end{aligned} \tag{2}$$

The nonlinear dynamic of the robot is presented in joint space in (3). The tri-axial joint flexibility is utilized to model the joint stiffness and damping [16], in order to account for the joint rotational bending, $q_{xy\,(12\times1)}$, in addition to the joints rotational deflection around their axis of actuation, $q_{z\,(6\times1)}$. The robot base's axial and bending rotational deflections are represented in $q_{b\,(3\times1)}$. To consider the joints motion along the identification trajectory, the joints motor positions $q_{m\,(6\times1)}$ are added to the degree of freedom (DOF) vector, $q_{(27\times1)}$.

$$\begin{aligned}
[\tau_m{}^T,\tau_{ext}{}^T]^T&=M(q)\ddot{q}+C(q,\dot{q})\dot{q}+\underbrace{(D+f_{vq})}_{C'}\dot{q}+Kq\\
q&=[q_m{}^T,q_z{}^T,q_{xy}{}^T,q_b{}^T]^T
\end{aligned} \tag{3}$$

where τ_m is the joints motor torque vector and τ_{ext} is the external torque vector. $M(q)$ is the inertia matrix and $C(q,\dot{q})$ is the Coriolis and centrifugal matrix. K is the stiffness matrix containing joints axial and bending rotational stiffness. D is the damping matrix incorporating joints axial and bending rotational damping. f_{vq} includes the viscous friction coefficients. C' is the total damping matrix, combining the joints damping and viscous friction terms. Gravitational torques and Coulomb friction, which are static torques, are neglected in this dynamic analysis. The load cell, spindle, tool holder, and tool are modeled as rigid lumped masses located at their centers of gravity. Robot dynamics in (3) is converted to Cartesian space using the Jacobian matrix $J(q)$, linearized, and transferred into frequency domain, as presented in (4).

$$\begin{bmatrix} F_x \\ F_y \\ F_z \end{bmatrix} = \underbrace{J(q)^{-T}(-\omega^2 M(q) + j\omega(C+C') + K)J(q)^{-1}}_{G} \begin{bmatrix} X \\ Y \\ Z \end{bmatrix} \quad (4)$$
$$\Rightarrow G \begin{bmatrix} X \\ Y \\ Z \end{bmatrix}$$

in which X, Y, and Z are Cartesian vibrations in the frequency domain. By reorganizing (4) and considering F_z=0 in the proposed identification method, the FRFs are derived in (5) and thereby extracted from the robot model, where G, defined in (4), is the inverse of FRF matrix H.

$$\begin{bmatrix} X \\ Y \\ Z \end{bmatrix} = G^{-1} \begin{bmatrix} F_x \\ F_y \\ 0 \end{bmatrix} = H \begin{bmatrix} F_x \\ F_y \\ 0 \end{bmatrix}, \; H = \begin{bmatrix} H_{xx} & H_{xy} & H_{xz} \\ H_{yx} & H_{yy} & H_{yz} \\ H_{zx} & H_{zy} & H_{zz} \end{bmatrix} \quad (5)$$

Since F_z=0, analyzing the z-direction vibration response involves evaluating only H_{zx} and H_{zy}. However, accurate prediction of H_{zz} is also essential for three-dimensional chatter prediction in robotic milling and drilling. Based on (5), in which $H_{zx}=G^{-1}{}_{31}$ and $H_{zy}=G^{-1}{}_{32}$, the last line of (2), representing the z-direction vibration response, can be written as:

$$\frac{Z}{A} = |G^{-1}{}_{31}|(\cos(\angle G^{-1}{}_{31}) + j\sin(\angle G^{-1}{}_{31})) + |G^{-1}{}_{32}|(\cos(\angle G^{-1}{}_{32} - \pi/2) + j\sin(\angle G^{-1}{}_{32} - \pi/2)) \quad (6)$$

$G^{-1}{}_{31}$ and $G^{-1}{}_{32}$ that contribute to z-direction vibration response can be calculated using the elements of G:

$$G^{-1}{}_{31} = \frac{G_{12}G_{23} - G_{13}G_{22}}{\det(G)}, \; G^{-1}{}_{32} = \frac{G_{11}G_{23} - G_{13}G_{21}}{\det(G)} \quad (7)$$

Based on (8) where H_{zz} is calculated, the elements G_{11}, G_{22}, G_{12} and G_{21} compose the numerator of H_{zz}, while det(G) serves as the common denominator for all transfer functions in H.

$$H_{zz} = G^{-1}{}_{33} = \frac{G_{11}G_{22} - G_{12}G_{21}}{\det(G)} \quad (8)$$

From (6), (7), and (8), it follows that by including the z-direction vibration response in the identification process, all four elements that compose the numerator of H_{zz} are taken into account and evaluated. This is a unique feature for z-direction prediction in this identification approach where F_z=0, and it can increase the accuracy of H_{zz} peaks prediction. For example, by examining the x or y vibration response, only two elements of the H_{zz} numerator are evaluated. These conclusions are experimentally validated in Section IV.

III. Input Force Investigation and Model Identification

A. Input Force Examination

This study uses both the theoretical input force from (1) and the force measured by a load cell to identify dynamic parameters and compare results. The robot is positioned at an arbitrary posture, as shown in Fig. 4(d) in Section IV. The load cell, mounted on the end effector, is affected by vibrations during excitation, influencing the measured values. The measured x- and y-direction forces in the time domain are shown in Fig. 2(a). Measured force signals in Fig. 2(a) exhibit resonant behavior as the centrifugal chirp sweeps through each natural frequency, indicating the influence of the robot's vibration modes on the measured forces. The relationship between the measured force and the actual imposed centrifugal force, based on the free body diagram of the spindle and tool, is expressed in (9).

$$F_{rec}(t) = F(t) + m_{sp}a_{sp} \quad (9)$$

where F_{rec} is the force vector measured by the load cell, shown in Fig. 2(a), and F is the applied chirp centrifugal force vector. m_{sp} is the combined spindle, tool holder and tool inertia. a_{sp} is

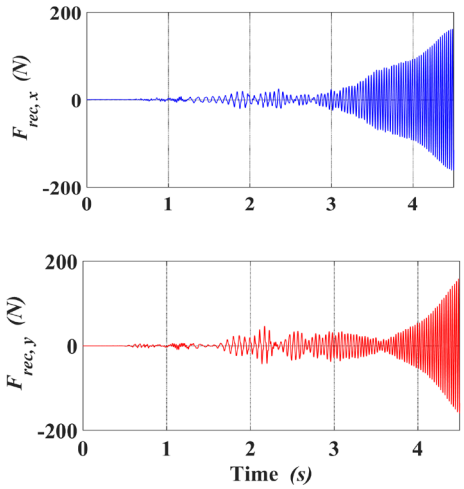

(a)

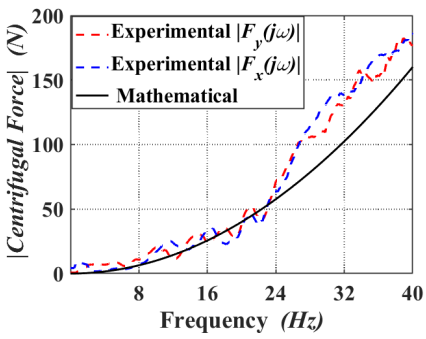

(b)

Figure 2. (a): Time domain measured forces before correction, (b) frequency domain experimental and mathematical forces.

the spindle acceleration vector measured by the accelerometer. The load cell inertia is neglected in this equation, compared to the combined spindle, tool holder, and tool inertia. Equation (9) is used for force correction and to obtain the experimental F. After conversion to the frequency domain, the resulting experimental F is plotted in Fig. 2(b) and compared to the mathematical force magnitude obtained using (1). Between 8 and 24 Hz, corresponding to the frequency range of the robot's vibration modes at the experiment's posture, the experimental forces exhibit oscillations due to these modes that cannot be fully corrected because of parameter uncertainties in (9). Above 24 Hz, a systematic discrepancy between the mathematical and corrected experimental forces arises from dynamic coupling between the robot's structure and the load cell, spindle, and offset mass tool mounted in series.

The mathematical and corrected experimental forces shown in Fig. 2(b) are both used in the *fast chirp* validation experiments in Section IV.A, and the resulting vibration responses are compared to a reference response.

B. *Parameter Identification considering Z-direction Vibration*

In this section, the joint stiffness and damping parameters are identified using the *fast chirp* identification method, the derived formulations, and the dynamic model of the industrial robot described in Section II. The robot moves continuously along the identification trajectory at a tool center point (TCP) speed of 10 mm/s. Four identification zones, corresponding to different robot joint poses, are selected where the robot is excited using the fast-chirp centrifugal force, and the input force and vibration responses are recorded. The experimental force obtained from corrected load cell data is used in this section. The TCP trajectory and identification zones are shown in Fig. 3(a), and the robot poses at these zones are depicted in Fig. 3(b). After obtaining the input and output data, as well as performing signal processing and calculations, the experimental vibration responses $(X/A,\ Y/A)_{Experimental}$, are obtained. Simulation vibration responses $(X/A,\ Y/A)_{Simulation}$ are computed using the mathematical model presented in (3)-(5) and the formulations introduced in (2). Following the parameter identification approach described in [12], the vibration responses in the x and y directions, corresponding to the axes where the excitation force is applied, are first incorporated into the identification process. The model parameters are identified by minimizing the deviation between the experimental and simulated normalized vibration responses using the "particleswarm" optimizer in MATLAB®.

TABLE I. IDENTIFICATION RESULTS

	Average Estimation Error (%)	
Zone Number	***Natural Frequency***	***Damping Ratio***
1	1.8	4.7
2	5.2	7.1
3	2.4	8.5
4	1.6	10.2

Using the identified model, the results of identification, including the average estimation error of the natural frequency and damping ratio across all modes of the normalized vibration responses, are summarized in Table I. The total average errors across all modes and zones are 2.7% for natural frequency estimation and 7.6% for damping ratio estimation. Evaluation of the identified model in a validation zone is performed in Section IV.B.

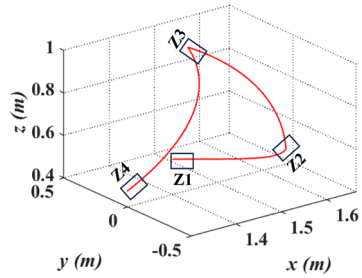

(a)

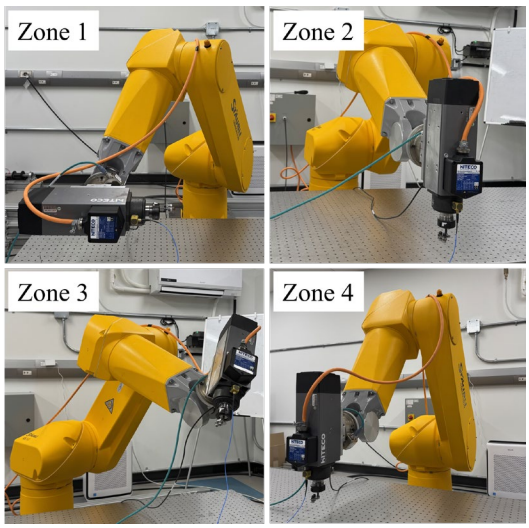

(b)

Figure 3. (a): TCP path during the identification, (b): Identification zones.

The primary objective of this paper is to improve the accuracy of the identified model in the z direction. As shown in the formulations in Section II.B, incorporating the z-direction vibration response to the centrifugal force applied in the x and y directions can enhance the model's performance in estimating z-direction dynamics. To experimentally validate this, the z-direction vibration response Z/A, is included in the identification process and the stiffness and damping parameters in the dynamic model are re-identified using the formulations presented in Sections II and III and the following cost function:

$$\textbf{\textit{Cost function}}:(zone\ i:1\ to\ 4)$$

$$\min_{K,\,C'} \sum_{i=1}^{n} \left\{ W_i(\omega).\left[\left| \left(\frac{X}{A},\frac{Y}{A},\frac{Z}{A}\right)_{i,\text{Simulation}} - \left(\frac{X}{A},\frac{Y}{A},\frac{Z}{A}\right)_{i,\text{Experiment}} \right| \right] \right\} \quad (10)$$

$W_i(\omega)$ is the weighting function to penalize the error around the vibration modes. Identifiable parameters are the joints stiffness and total damping matrices K and C', as defined in

(3). Inertial parameters included in inertia and Coriolis and centrifugal matrices are considered known based on an inertia and friction nonlinear identification method [3]. The impact of including the z-direction vibration response on predicting z-dynamics and H_{zz} is experimentally examined and discussed in Section IV.C.

IV. Validation of Identification and Z- Dynamics Estimation

In this section, the obtained normalized vibration displacements in response to the fast-chirp excitation, using both the mathematical and experimental forces, are first compared and validated. Then, the identified model is validated in a new zone. Finally, using the enhanced identified model, the prediction results in the z direction are presented to assess the improvement in z-dynamics prediction accuracy.

A. Validation of Vibration Responses in All Directions using Mathematical and Experimental Excitation Forces

In this section, the robot is excited in a new zone, referred to as the validation zone, which is not included in the identification trajectory of Section III. The robot posture in this zone is shown in Fig. 4(d). During excitation, the robot moves with a tool center point (TCP) speed of 10 mm/s. The magnitudes of the normalized vibrations in the x, y, and z directions, denoted as X/A, Y/A and Z/A respectively, are shown in Fig. 4(a–c). To normalize the displacements, the recorded data is divided by the force magnitude A. As described in Section III.A and shown in Fig. 2(b), A is calculated both mathematically using (1) and experimentally using the load cell measurements, corrected with (9), to obtain the experimental A. The magnitudes of the vibration responses in Fig. 4 are obtained using both the mathematical and experimental A, and the results are compared. The reference in this figure, denoted as "Hammer-based", is the simulated response obtained using (2), where hammer tests in a quasi-static situation [5] are employed to determine the direct and cross dynamic FRFs. The quasi-static hammer test allows the moving joints' frictional behavior to be considered in the reference data.

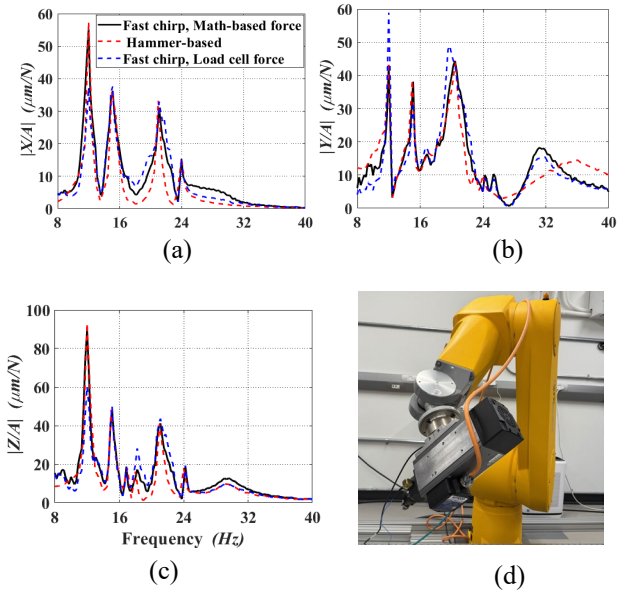

Figure 4. (a)-(c): Fast chirp normalized vibration responses validation and comparisons, (d) Robot posture in the validation zone.

The results demonstrate that in the low-frequency range below 24 Hz, the mathematical force-based vibration responses are closer to the reference, whereas at frequencies above 24 Hz, the experimental force-based vibrations show better agreement with reference. These observations are consistent with the input force investigation findings discussed in Section III.A. In the experimental results presented in the following sections, to improve validation accuracy, the mathematical force is used to normalize the vibration responses below 24 Hz, while the experimental force is used for frequencies above 24 Hz.

B. Validation of Identified Model

To experimentally evaluate the identified model from Section III before considering z-direction vibrations in the identification process, the model is used to predict the vibration responses in the validation zone. The simulated normalized vibration magnitudes are compared with the experimental fast-chirp vibration responses in Fig. 5(a–c). The results show that the identified model predicts the magnitudes of the x-direction vibration peaks at 12, 15, 21, and 24 Hz modes with an average error of 10.3%. For the y-direction vibrations, it predicts the 12, 15, 20.5, and 30 Hz modes with an average error of 9.7%. For the z-direction vibration response, the model accurately predicts the magnitudes at the 12 and 24 Hz modes, while the accuracy decreases for the 15 and 21 Hz modes, resulting in an average error of 18%. The model also fails to estimate the smaller peaks at 17, 18.2, and 29 Hz. The comparison between the simulated H_{zz}, extracted from the identified model, and the H_{zz} obtained from quasi-static hammer test is shown in Fig. 5(d). The average error in predicting the magnitude of the H_{zz} modes is 25.7%.

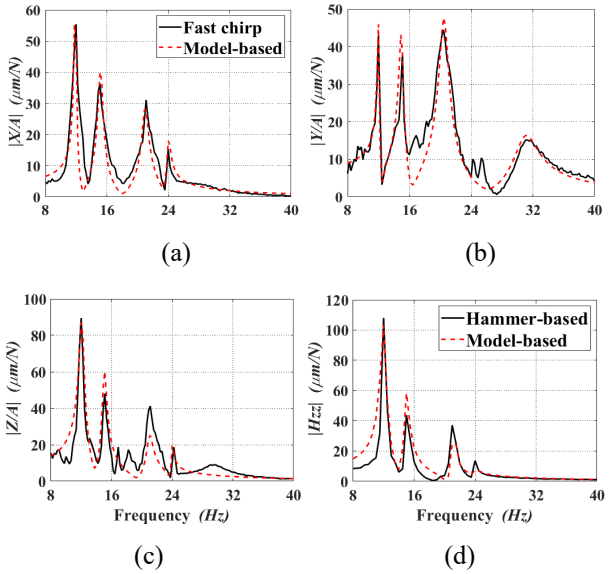

Figure 5. Parameter identification validation results in the new zone. (a)-(c): normalized vibration responses, (d): H_{zz}.

According to the results in Fig. 5, the model accuracy in the x and y directions is higher than in the z direction. The errors in the z-direction estimations are attributed to the fact that the robot cannot be excited directly in this direction, and

the z vibration responses were not considered in the identification process at this stage.

C. Validation of Improved Z-direction Prediction

After including the z-direction vibrations and updating the identified parameters using (10), the improved model is used to predict the vibration response Z/A, and H_{zz}. As illustrated in Fig. 6, these results are compared with those in Fig. 5. The normalized z-direction vibration responses in Fig. 6(a) show an 82% improvement in model accuracy for predicting the peaks at 15 Hz and 21 Hz. Furthermore, the improved model was able to estimate the smaller peaks at 17 Hz and 29 Hz, while the smaller peak at 18.2 Hz remains unpredicted. According to these results, incorporating Z/A response in the identification process mainly improves the estimation of vibration peaks that arise from the contribution of the z-direction cross FRFs, H_{zx} and H_{zy} in the z dynamics. Fig. 6(b) shows that extracted H_{zz} from the improved model. The results indicate that the average error in predicting the magnitude of the H_{zz} vibration modes is 12.9%, representing a 49.8% error reduction compared to the previously identified model, in which the z-direction vibration responses were not considered.

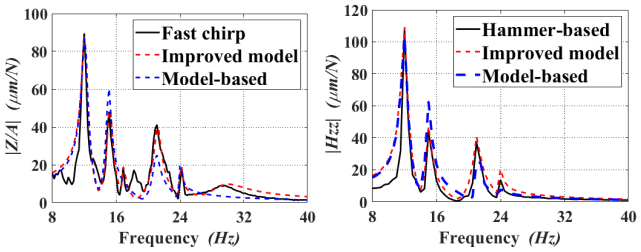

(a) (b)

Figure 6. z-direction dynamics prediction improvement results. (a): normalized vibration responses, (b): H_{zz}.

V. Conclusion

A novel joint dynamic parameter identification method using *fast chirp* centrifugal force excitation has been proposed and experimentally validated in this study, with a focus on improving the prediction of z-direction dynamics. A potential application of this approach lies in robotic operations involving high force and vibration, where precise modelling of z-direction dynamics is essential for reliable three-dimensional chatter stability prediction, especially in processes like milling and, more notably, robotic drilling, which is subject to high-amplitude forces along the z-axis. Future work will concentrate on the sensitivity of z-direction estimation to further improve accuracy, including the design of optimized identification trajectories.

Acknowledgment

The authors would like to acknowledge the Natural Sciences and Engineering Research Council of Canada (NSERC), and Alberta Innovates (AI) for funding this work.

References

[1] W. Ji and L. Wang, "Industrial robotic machining: a review", *International Journal of Advanced Manufacturing Technology*, vol. 103, pp. 1239–1255, 2019.

[2] J. Wu, J. Wang, and Z. You, "An overview of dynamic parameter identification of robots", *Robotics and Computer-Integrated Manufacturing*, vol. 26, pp. 414–419, 2010.

[3] A. Khishtan, S. H. Kim, and J. Lee, "A hybrid model in a nonlinear disturbance observer for improving compliance error compensation of robotic machining", *Robotics and Computer-Integrated Manufacturing*, vol. 92, 102887, 2025.

[4] M. Grotjahn, M. Daemi, and B. Heimann, "Friction and rigid body identification of robot dynamics", *International Journal of Solids and Structures*, vol. 38, pp. 1889–1902, 2001.

[5] L. T. Tunc and B. Gonul, "Effect of quasi-static motion on the dynamics and stability of robotic milling", *CIRP Annals*, vol. 70, no. 1, pp. 305–308, 2021.

[6] S. Moberg, S. Hanssen, E Wernholt, and T. Brogardh, "Modeling and Parameter Estimation of Robot Manipulators Using Extended Flexible Joint Models", *Journal of Dynamic Systems, Measurement, and Control*, vol. 136, 031005-2, 2014.

[7] X. Mao, Y. Chen, T. Ma, J. Guo, X. Yuan, N. Jiang, Y. Xu, L. Zhang, X. Tang, and Y. Peng, "Output-only complete mode shape identification of milling robot body structures using a limited number of current sensors", *CIRP Journal of Manufacturing Science and Technology*, vol. 53, pp. 48–66, 2024.

[8] M. Newman and M. Khoshdarregi, "Automatic structural identification and vibration suppression of industrial robots using a custom active damper", *2022 22nd International Conference on Control, Automation and Systems (ICCAS)*, pp. 1033–1038.

[9] K. Wu and B. Kuhlenkoetter, "Experimental analysis of the dynamic stiffness in industrial robots", *Applied Sciences*, vol. 10, no. 23, 8332.

[10] Y. P. Liu and Y. Altintas, "In-process identification of machine tool dynamics", *CIRP Journal of Manufacturing Science and Technology*, vol. 32, pp. 322–337, 2021.

[11] V. Nguyen and S. Melkote, "Identification of industrial robot frequency response function for robotic milling using operational modal analysis", *Procedia Manufacturing*, vol. 48, pp. 154–158, 2020.

[12] J. Lee and A. Khishtan, "Automated identification of joints dynamic parameters in moving industrial robots for milling applications", *CIRP Annals*, vol. 74, no. 1, pp. 487–491, 2025.

[13] C. Qin, Y. Sun, J. Tao, H. Zeng, Y. Li, and C. Liu, "A Chatter Recognition Approach for Robotic Drilling System Based on Synchroextracting Chirplet Transform", *IEEE Sensors Journal*, vol. 23, no. 22, pp. 27670–27678, 2023.

[14] Y. Altintas, "Analytical prediction of three dimensional chatter stability in milling", *JSME International Journal*, vol. 44, no. 3, pp. 717–723.

[15] M. Cordes, W. Hintze, and Y. Altintas, "Chatter stability in robotic milling", *Robotics and Computer-Integrated Manufacturing*, vol. 55, pp. 11–18, 2019.

[16] H. N. Huynh, H. Assadi, E. Riviere-Lorphevre, O. Verlinden, and K. Ahmadi, "Modelling the dynamics of industrial robots for milling operations", *Robotics and Computer-Integrated Manufacturing*, vol. 61, no. 4, 101852, 2020.